Research Article

Effect of annealing temperature on corrosion properties of rolled AZ31-Ce magnesium alloy

Fangkun Ning[1] · Qichi Le[1] · Shuping Kong[1]

Received: 6 January 2020 / Accepted: 2 March 2020 / Published online: 26 March 2020

Abstract
The corrosion properties of rolled AZ31 magnesium alloy addition Ce before and after annealing at different rolling temperatures (200 °C, 250 °C, 300 °C and 350 °C) and the corrosion resistance and surface morphology of different sections of the samples were studied. The results showed that the corrosion rate and weight loss of the plate without annealing were higher than that of the plate after annealing. The corrosion resistance of the transverse direction–normal direction (TD–ND) cross section was the most, and the corrosion pits after annealing were shallower than that of unannealed samples. The low Ce element content can improve the corrosion resistance of magnesium alloy. In addition, the above properties were the best at 200 °C whether annealed or not.

Keywords Magnesium alloy · Corrosion resistance · Rolling · Annealing · Grain size

1 Introduction

Magnesium and alloys have attracted considerable recent attention and have great potential in industrial applications [1, 2], especially in aerospace and transportation fields due to their suitable mechanical properties and high strength to weight ratios [3, 4]. However, magnesium alloys exhibit poor corrosion properties and tolerable formability [5, 6]. One of the promising methods for increasing strength and formability is refining microstructural. The material with fine grains has a more grain boundary to hinder dislocation movement. But more grain boundaries store more energy, which makes the material more possible to be corroded [7, 8]. Appropriate annealing can eliminate internal stress and distortion energy at grain boundary. Annealing includes full annealing and stress relief annealing, which full annealing making the grain recrystallize or even grow up and increase the plastic and decrease the strength of the material [9, 10]. The stress relief annealing can not only reduce or dispel the residual stress produced in cold and hot working and forming of deformed magnesium alloy products, but also eliminate the residual stress in castings or ingots [11, 12]. In the rolling process of magnesium alloy sheet, the grain size and shape of each section are very different due to the various stress on diverse cross sections. Rare earth elements have valence electron and distinctive atomic structures. Wrought magnesium alloys with Ce addition can enhance the mechanical properties at ambient and high temperatures and improve corrosion resistance [13]. Hamu et al. [14] studied the relation between severe plastic deformation microstructure and corrosion behavior of AZ31 magnesium alloy. The relation can be explained by the effects of the process on microstructure of AZ31 Mg alloy such as grain size and dislocation density caused by the change in recrystallization behavior. Song et al. [15] investigated the effect of microstructure change on corrosion behavior of ECAPed AZ91D Mg alloy. The ECAPed alloy with ultra-fine grains displays a significantly lower corrosion resistance. Hama et al. [16] performed two-step loading tests on AZ31

✉ Qichi Le, qichil@mail.neu.edu.cn | [1]Key Laboratory of Electromagnetic Processing of Materials, Ministry of Education, Northeastern University, Shenyang 110819, China.

rolled magnesium alloy sheet with strong basal texture in ND (normal direction). The texture evolution of the sheet in different direction was investigated. Mg-Zn-Ca alloys as biodegradable implant materials have become a hot spot [17]. However, they have a rapid degradation rate in the body and cannot maintain the mechanical properties for a long time. Therefore, grain refinement and texture control are used as methods to improve corrosion resistance of magnesium alloys. Op'T et al. [18] studied the corrosion of pure magnesium with different grains and electrochemical tests in NaCl solution. According to the change of current density and weightlessness, it could be seen that the corrosion resistance of pure magnesium in NaCl solution was enhanced with the decrease of grain size. Leil et al. [19] found that, when the alloy component is not changed, the corrosion characteristic of the magnesium alloy is closely related to the grain size and the number and distribution of the intermetallic compound. Kim et al. [20] investigated that the deformation of the magnesium alloy through the ECAP, the elongation is obviously increased, but the strength is decreased, which is mainly due to the weakening of the texture formed by the extrusion process and the strengthening effect of the grain refinement. Song et al. [21] indicated that hot rolling could refine the grain size of magnesium alloy and change the grain orientation. The grain boundary acts as a corrosion barrier and thus an alloy with small grain size has more such barriers to passivate the alloy surface, whereas an alloy with large grain size does not. In the corrosion structure of AZ31 magnesium alloy, the outer layer is composed of Mg $(OH)_2$, and the inner layer is composed of Al_2O_3 and MgO. The unstable MgO in the inner layer will react with H_2O to form Mg $(OH)_2$. When Ce element is added to the alloy, the structure model of the corrosion layer will change. Because Ce has a strong affinity with O, Ce_2O_3 will be generated. Due to the low chemical activity of Ce2O3 and its insensitivity to NaCl corrosive medium, Ce_2O_3 can act as a passivating film, thus improving the corrosion resistance of the alloy.

In this paper, the corrosion behavior especially weight loss of different cross sections of AZ31-Ce sheet before and after annealing under different rolling conditions is studied in order to determine quickly the influence of heat treatment on the plane corrosion of samples and provide guidance in anticorrosion and use of magnesium alloy sheet.

2 Materials and methods

The alloy was prepared by direct electrical resistance melting in a mild steel crucible at 710 °C. Flux of 0.5% SF6 (volume fraction) + CO2 was also used to purify the melt, as well as prevent it from burning. AZ31-Ce blank with a chemical composition of Mg-3.5% Al-0.35% Zn-0.21% Ce (in wt. %) fabricated through self-developed low-frequency electromagnetic semi-continuous casting (LFEC) technology [22] and homogenized were used in these experiments. High quality Mg alloy ingots with smooth surface and excellent metallurgical quality were achieved by the way of LFEC (see Fig. 1).

The billet was manufactured to rectangular samples of 150 × 80 × 10 mm and rolled at the rolling mill of Φ260 × 400 mm work rolls. The rolling process was shown in Table 1. After rolling, the specimens with cross section

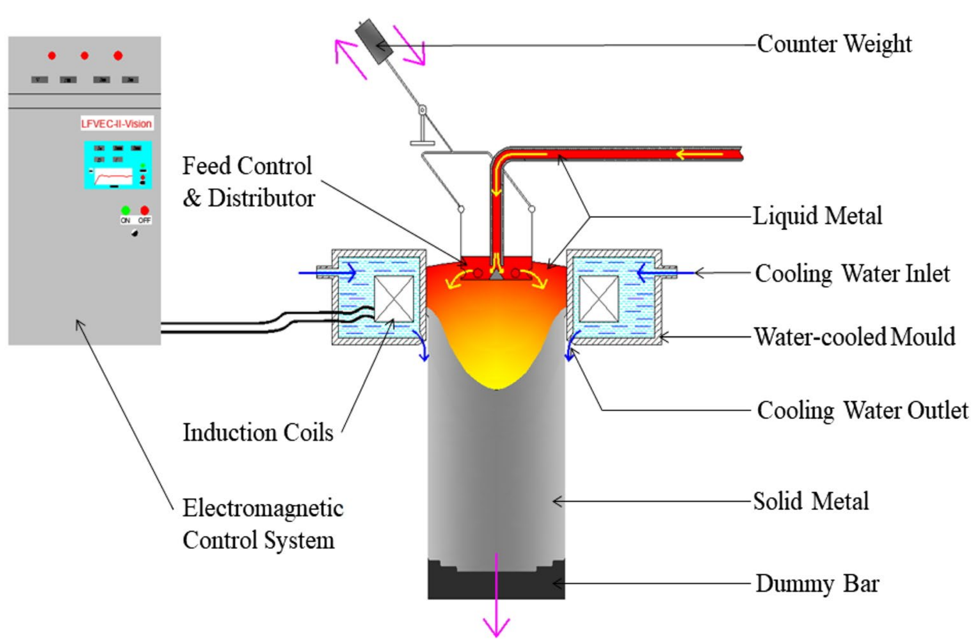

Fig. 1 Schematic diagram of low-frequency electromagnetic semi-continuous casting

Table 1 Experimental scheme of hot rolling

No. of plate	1	2	3	4	5	6
Temperature (°C)	200	250	300	350	350	350
Rolling reduction (%)	40	40	40	40	25	60
Rolling speed (r/min)	21	21	21	21	21	21

of 10 × 10 mm were cut out in the same position of the sheet. One part was heat treated at 350 °C for 30 min and the other part was not done annealing. The six surfaces of specimens were polished with 2500# sand paper and immersed into the 3.5% NaCl solution for 5 days (see Fig. 2). After corrosion, the specimen was washed in chromic acid solution by ultrasonic cleaning machine for 10 min. The specimen was weighed before and after corrosion and the morphology of RD–TD, RD–ND and TD–ND surfaces were observed by OM (Leica DMR) and SEM (SHIMADZU SSX-550), respectively. Weightlessness, uncorroded area ratio and corrosion rate were calculated to characterize intuitively corrosion property of each surface.

3 Results and discussions

3.1 Microstructure

The corrosion behavior of AZ31-Ce alloy is mainly determined by its microstructure, second phase size, number and distribution. Thus, it is significant to analyze the microstructure of AZ31-Ce under various conditions. It's helpful to obtain a thorough understanding of the relationship between the corrosion behavior and microstructure.

Figure 3 displays the optical metallographic images of AZ31-Ce alloy under different conditions.

The rolled sheet is not heat treated (Fig. 3a–d), whilst the other sheet is disposed at 350 °C for 30 min (Fig. 3e–h). The sheet is rolled at 200 °C (Fig. 3a and e), 350 °C, 40% rolling reduction and 21 rpm rolling rate (Fig. 3b and f), 60% rolling reduction (Fig. 3c and g) and 7 rpm rolling rate (Fig. 3d and h). There are more deformed structure, which containing shear bands and twins in the no heat treated rolled sheet. The shear band are composed of fine grains, and twins are produced when deformation is difficult to carry out. The texture of the basal surface of AZ31-Ce magnesium alloy is very strong, and its orientation is not conducive to the activation of basal slip. The deformation will be concentrated inside the shear bands once formed, while the part outside the shear bands emerge small degree of deformation due to the unfavorable orientation. Therefore, several long shear bands will be produced in the low temperature rolling process, which is the result of strain concentration. When rolling at higher temperature, both prismatic slip and pyramidal slip can be activated to cancel and rearrange the dislocations, which relieve the stress concentration to a certain extent and delay the occurrence of the strain concentration and the shear bands.

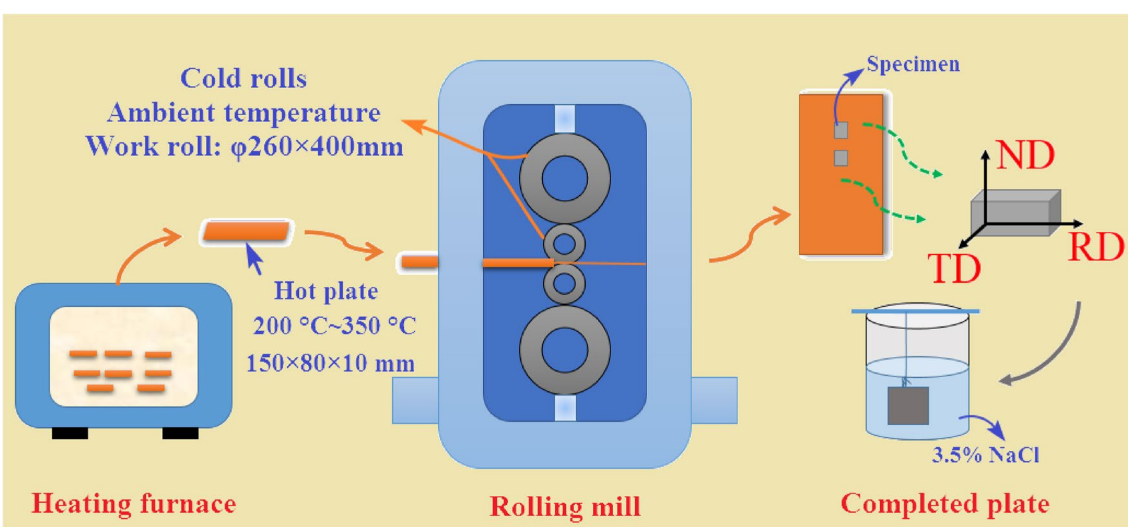

Fig. 2 Schematic diagram of rolling mill, plate size and corrosion specimen

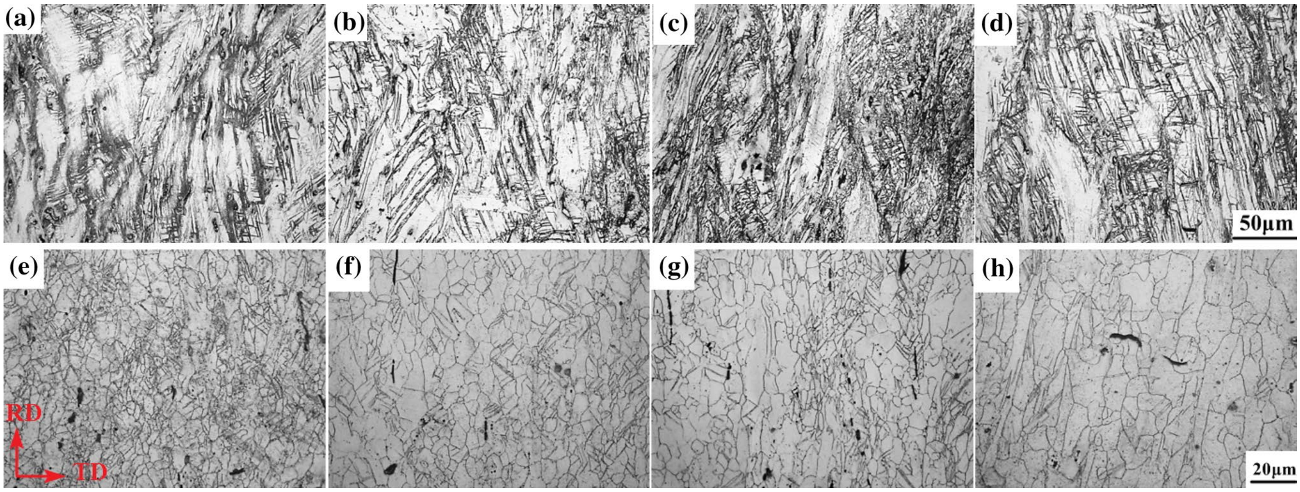

Fig. 3 Optical metallographic microstructures of AZ31-Ce alloy under diverse conditions, HT-annealing: **a** 200 °C rolled alloy, No HT **b** 350 °C rolled alloy, No HT **c** 60% rolling reduction alloy, No HT **d** 7 rpm rolling rate alloy, No HT **e** 200 °C rolled alloy, HT **f** 350 °C rolled alloy, HT **g** 60% rolling reduction alloy, HT **h** 7 rpm rolling rate alloy, HT

The recrystallization grains are observed in the sheet after HT, but the grain size of each condition is different. The grain size of the sheet rolled at 200 °C is less than 10 μm (Fig. 3e), while the grain sizes are more than 10 μm (Fig. 3f–h). When the plate is rolled at lower temperature (200 °C, Fig. 3a), there are more distortion energy stored in the microstructure. After annealing, the distortion energy release makes the particles nucleate and grow up in many places, and the grain size is small. When the sheet is rolled under large reduction (60%, Fig. 3c), the grain is seriously broken, a large amount of distortion energy is stored in the microstructure, and the degree of grain recrystallizing is low. Zhi et al. [23] indicated that after rolling under high pressure, shear bands composed of a large number of fine grains was formed along the TD and parallel to the RD. Jia et al. [24] indicate that when the material rolled at lower speed (7 rpm in this paper, Fig. 3d), the twin was mainly composed of the parallel twin and the intersecting twin and the microstructure had less recrystallization. That is the recrystallizing nucleation mechanism is influenced and controlled by the plastic deformation mechanism [25]. Besides, the plastic deformation mechanism is affected by the rolling process.

The addition of Ce element to the AZ31 alloy can refine the structure and break the coarse β phase with a fine dispersion state. As shown in Fig. 4, the second phase particles are mostly distributed at the grain boundary, and individual larger particles are distributed in the matrix. EDS analysis of point 1 and 2 shows that white particles contain Ce element. The atomic percent of Al and Ce elements is about 11–3, so the second phase is $Al_{11}Ce_3$. The corrosion resistance of AZ31 alloy can be improved owing to adding Ce. The potential difference between Al–Ce phase rich in rare earth and aluminum elements and α-Mg matrix is smaller than that between β-$Mg_{17}Al_{12}$ and α-Mg matrix [26]. Therefore, addition of Ce can improve the corrosion resistance of AZ31 magnesium alloy in 3.5% NaCl solution.

3.2 Corrosion rate and corroded surface morphology

The number of precipitated intermetallic particles and the densities of twins could be changed during annealing. Song eta al. [27]. indicated that the diversion of corrosion behavior in response to annealing cannot be the same for kind of alloy surfaces. After the magnesium alloy rolled by various processes, the corrosion of each surface needs to be comprehended before being used due to the difference in grain size and the misorientation in each section.

After the sample is corroded, the uncorroded area and weightlessness of each section are counted. Figure 5 is the SEM graph (a), OM of blaze (b) and area calibration (c) of corroded surface morphology of RD–TD cross section rolled at 300 °C. The red zones in Fig. 5a are uncorroded surfaces, which are the white points in Fig. 5b. Image Pro Plus (IPP) software is adopt to statistic the area of the white points (Fig. 5c). Corrosion rate and weightlessness percentage of rolled sheet at different temperatures with HT and without HT are shown in Fig. 6. The corrosion rate could be described with the following formula,

$$I = \frac{m_0 - m_1}{t \cdot \sum_{x=1}^{6} S_x} \quad (1)$$

where I is the corrosion rate (mg/d cm^2), m_0 is the weight of specimen before immersion, m_1 is the weight of specimen

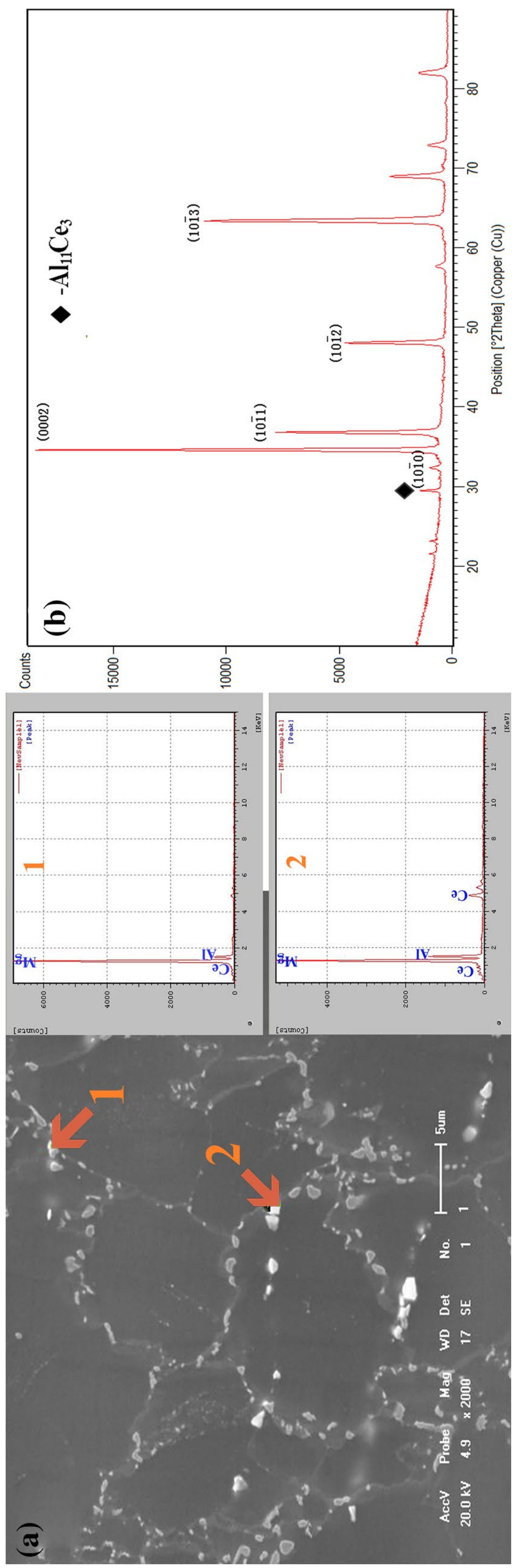

Fig. 4 **a** SEM micrograph of 350 °C rolled alloy with HT and EDS analysis of point 1 and 2, **b** XRD analysis of AZ31 sheet

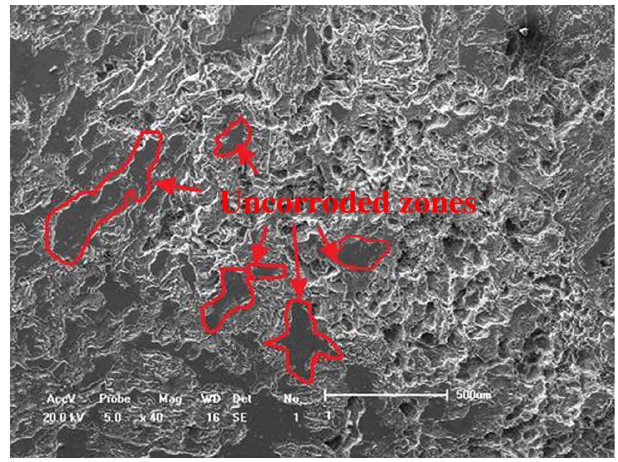

Fig. 5 SEM graph of corroded surface morphology, 300 °C RD–TD cross section as an example

after immersion, S is the one of the exposed area of the specimen, and t is immersion time.

The corrosion rate of rolled sheet without HT fluctuate greatly with temperature. This is related to the grain size and stored distortion energy of the sheet after rolling. The corrosion rate turns faster with the larger grain size and higher distortion energy. In addition, the low deformation temperature and large deformation resistance would make the second phase distribution in the matrix not uniformed, which caused the variety of corrosion rate. However, the corrosion rate of rolled sheet with HT increase with the augment of temperature, but decreases at 350 °C. At 350 °C, the higher degree of recrystallizing, the minor distortion energy stored in the material, and the coarser grain size after annealing lead to the decrease of corrosion rate. When the α-Mg phase and the β-$Mg_{17}Al_{12}$ phase constitute a galvanic cell, the β-$Mg_{17}Al_{12}$ phase will promote the corrosion of α-Mg phase. The corrosion of α-Mg phase can be reduced by reducing the content of β-$Mg_{17}Al_{12}$ phase. When rare earth Ce is added to AZ31 magnesium alloy, the Al atomic weight is consumed due to the formation of a new phase, $Al_{11}Ce_3$, which results in a decrease in the content of β phase. Moreover, the $Al_{11}Ce_3$ phase can act as an anode block.

Figure 7 is corroded surface morphology of each cross section at various temperature with HT and without HT. The area percentage after corroded of each cross section at different temperatures is counted, and the results are shown in Fig. 8a. It can be seen from the Fig. 8 that TD–ND section has the most remaining area after corrosion, which indicates that TD–ND section has the best corrosion resistance. The rolled sheet mainly consisting of closely packed crystallographic plane (0001) and deformation structure will emerge crystallization and become equiaxed crystal after HT, which changed

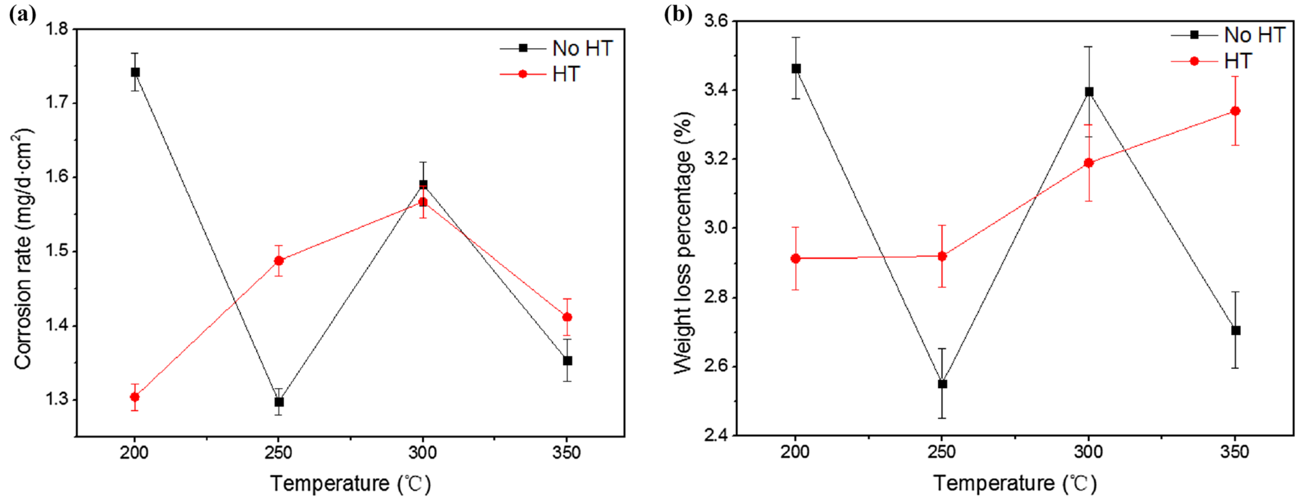

Fig. 6 **a** Corrosion rate and **b** weightlessness percentage of rolled sheet at different temperatures with HT and without HT

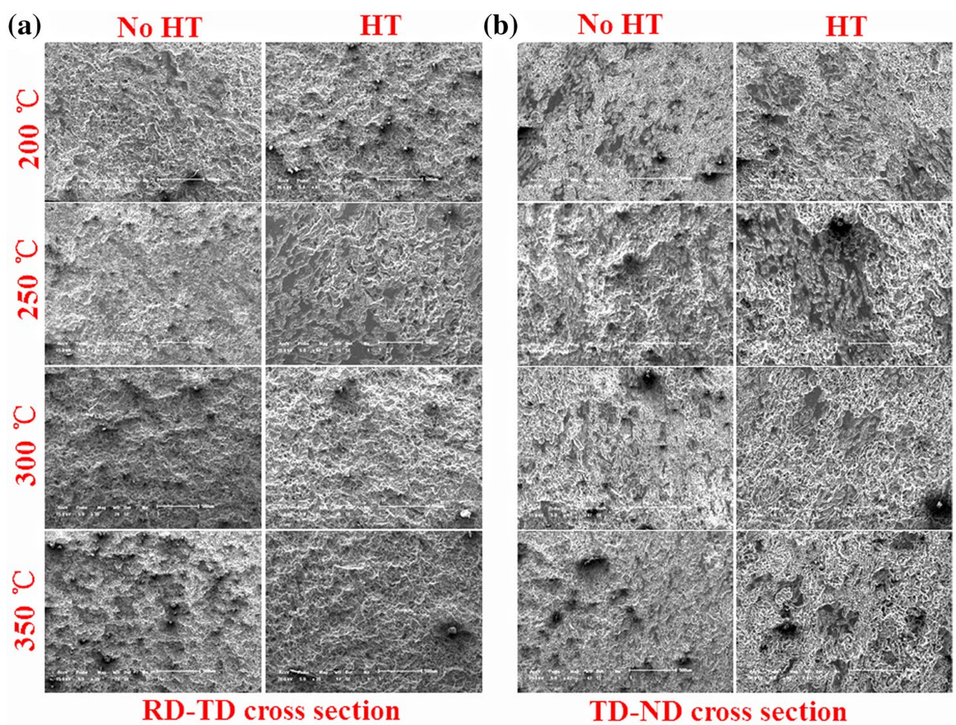

Fig. 7 Corroded surface morphology of different cross section at various temperature with HT and without HT **a** RD–TD, **b** TD–ND

the anodic and cathodic reaction activities. Figure 8b is the schematic diagram of grain size and morphology with different cross sections. The grains at the TD–ND cross section are fine and uniformed with lower surface energy. Grain refinement makes the grain boundaries increase in the alloy, and a large number of grain boundaries can be used as a barrier to prevent the corrosion. For the alloy after annealing, the corrosion rate descends with the decrease of rolling temperature, the corrosion resistance of RD–TD section is the worst, while the corrosion resistance of TD–ND section is the best. For RD–TD section, the corrosion resistance of no heat treated alloy is better than that of annealing. For the RD–ND and TD–ND section, the opposite is true of the above.

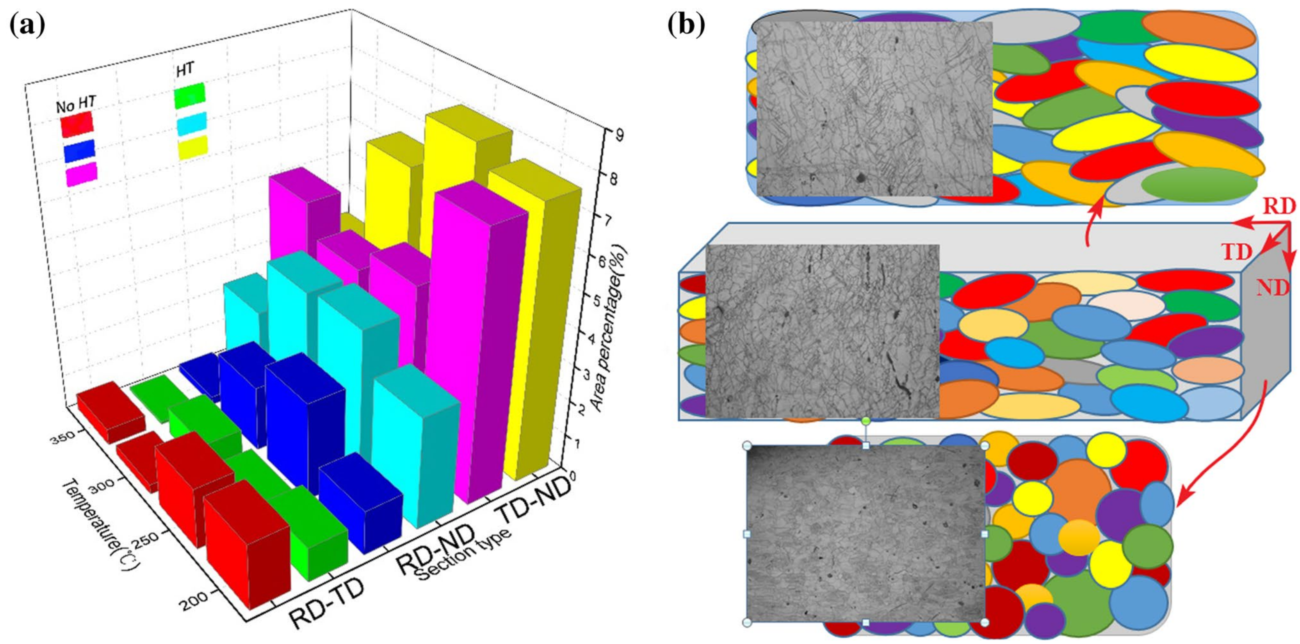

Fig. 8 **a** Area percentage after corroded of each cross section at different temperatures, **b** schematic diagram of grain size and morphology with different cross sections

4 Conclusions

The corrosion properties of each cross section of AZ31 magnesium alloy containing Ce before and after annealing at different rolling temperatures (200 °C, 250 °C, 300 °C and 350 °C) and the corrosion resistance and surface morphology of different sections of the samples were studied by immersing in 3.5 wt.% NaCl solution.

The sheet without annealing consisting of large numbers of twins, shear bands and distortional energy has worse corrosion resistance. For the alloy after annealing, the corrosion rate descends with the decrease of rolling temperature, the corrosion resistance of RD–TD across section is the worst, while the corrosion resistance and uncorroded area of TD–ND across section is the best. The ensemble weight loss of the sample rolled at 200 °C is least.

Acknowledgements This work was financially supported by the project from the National Key Research and Development Program of China (No. 2016YFB0301104), and National Natural Science Foundation of China (No. 51771043). The authors are grateful for supported by State Key Laboratory of Baiyunobo Rare Earth Resource Researches and Comprehensive Utilization.

Compliance with ethical standards

Conflict of interest The authors declare that they have no conflict of interest.

References

1. Jia W, Ma L, Tang Y, Le Q, Fu L (2016) Relationship between microstructure and properties during multi-pass, variable routes and different initial temperatures hot flat rolling of AZ31B magnesium alloy. Mater Des 103:171–182. https://doi.org/10.1016/j.matdes.2016.04.067
2. Pan FS, Yang MB, Zhang DF, Wang LY, Ding PD (2005) Research and development of wrought magnesium alloys in China. Mater Sci Forum 488–489:413–418. https://doi.org/10.4028/www.scientific.net/MSF.488-489.413
3. Yin SM, Wang CH, Diao YD, Wu SD, Li SX (2011) Influence of grain size and texture on the yield asymmetry of Mg–3Al–1Zn alloy. J Mater Sci Technol 27(1):29–34. https://doi.org/10.1016/S1005-0302(11)60021-2
4. Guo L, Chen Z, Gao L (2011) Effects of grain size, texture and twinning on mechanical properties and work-hardening behavior of AZ31 magnesium alloys. Mater Sci Eng, A 528(29):8537–8545. https://doi.org/10.1016/j.msea.2011.07.076
5. Padekar BS, Raja VS, Raman RKS, Lyon P (2013) Stress corrosion cracking behavior of magnesium alloys EV31A and AZ91E. Mater Sci Eng, A 583:169–176. https://doi.org/10.1016/j.msea.2013.06.085
6. Yin Z, Liu F, Song D, He S, Lin J, Yu F (2018) Stress corrosion cracking of a forged Mg–Al–Zn alloy with different surface conditions. J Chem. 2018:1–8. https://doi.org/10.1155/2018/4262860
7. Xie H, Jiang Z, Yuen WYD (2011) Analysis of microstructure effects on edge crack of thin strip during cold rolling. Metall Mater Trans B 42(6):1244–1252. https://doi.org/10.1007/s11663-011-9540-3
8. Ktari A, Antar Z, Haddar N, Elleuch K (2012) Modeling and computation of the three-roller bending process of steel sheets. J Mech Sci Technol 26(1):123–128. https://doi.org/10.1007/s12206-011-0936-4

9. Jia W, Tang Y, Le Q, Cui J (2017) Air-cooling analysis of AZ31B magnesium alloy plate: experimental verification, numerical simulation and mathematical modeling. J Alloys Compd. 695:1838–1853. https://doi.org/10.1016/j.jallcom.2016.11.017
10. Máthis K, Horváth K, Farkas G, Choe H, Shin K, Vinogradov A (2018) Investigation of the microstructure evolution and deformation mechanisms of a Mg–Zn–Zr–RE twin-roll-cast magnesium sheet by in situ experimental techniques. Materials 11(2):200. https://doi.org/10.3390/ma11020200
11. Tang Y, Jia W, Liu X, Le Q, Cui J (2017) Precipitation evolution during annealing of Mg–Li alloys. Mater Sci Eng, A 689:332–344. https://doi.org/10.1016/j.msea.2017.02.035
12. Mola R, Mróz S, Szota P, Sawicki S (2015) Analysis of the deformability of two-layer materials az31/eutectic/analiza możliwości odkształcania plastycznego materiału dwuwarstwowego AZ31/Eutektyka. Arch Metall Mater 60(4):3017–3022. https://doi.org/10.1515/amm-2015-0482
13. Zhu Y, Hu M, Wang D, Xu H, Wang Y, Ji Z (2018) Microstructure and mechanical properties of AZ31-Ce prepared by multipass solid-phase synthesis. Mater Sci Technol 34(7):876–884. https://doi.org/10.1080/02670836.2017.1412008
14. Hamu GB, Eliezer D, Wagner L (2009) The relation between severe plastic deformation microstructure and corrosion behavior of AZ31 magnesium alloy. J Alloys Compd. 468(1):222–229. https://doi.org/10.1016/j.jallcom.2008.01.084
15. Song D, Ma AB, Jiang JH, Lin PH, Yang DH, Fan JF (2011) Corrosion behaviour of bulk ultra-fine grained AZ91D magnesium alloy fabricated by equal-channel angular pressing. Corros Sci 53(1):362–373. https://doi.org/10.1016/j.corsci.2010.09.044
16. Hama T, Tanaka Y, Uratani M, Takuda H (2016) Deformation behavior upon two-step loading in a magnesium alloy sheet. Int J Plast 82:283–304. https://doi.org/10.1016/j.ijplas.2016.03.009
17. Gu X, Zheng Y, Zhong S, Xi T, Wang J, Wang W (2010) Corrosion of, and cellular responses to Mg–Zn–Ca bulk metallic glasses. Biomaterials 31(6):1093–1103. https://doi.org/10.1016/j.biomaterials.2009.11.015
18. op't Hoog C, Birbilis N, Estrin Y et al (2008) Corrosion of pure Mg as a function of grain size and processing route. Adv Eng Mater 10(6):579–582. https://doi.org/10.1002/adem.200800046
19. Abu Leil T, Hort N, Dietzel W et al (2009) Microstructure and corrosion behavior of Mg–Sn–Ca alloys after extrusion. Trans Nonferrous Met Soc China 19(1):40–44. https://doi.org/10.1016/S1003-6326(08)60225-3
20. Kim WJ, Hong SI, Kim YS, Min SH, Jeong HT, Lee JD (2003) Texture development and its effect on mechanical properties of an AZ61 Mg alloy fabricated by equal channel angular pressing. Acta Mater 51(11):3293–3307. https://doi.org/10.1016/S1359-6454(03)00161-7
21. Song G-L, Mishra R, Xu Z (2010) Crystallographic orientation and electrochemical activity of AZ31 Mg alloy. Electrochem Commun 12(8):1009–1012. https://doi.org/10.1016/j.elecom.2010.05.011
22. Le Q, Zhang Z, Cui J (2009) Effects of electromagnetic field and lubricate condition on the surface quality of magnesium alloy billet during LFEC processing. Sci China Ser E: Technol Sci 52(1):180–185. https://doi.org/10.1007/s11431-008-0294-3
23. Zhi C, Ma L, Huang Q, Huang Z, Lin J (2018) Improvement of magnesium alloy edge cracks by multi-cross rolling. J Mater Process Technol 255:333–339. https://doi.org/10.1016/j.jmatprotec.2017.12.022
24. Jia W, Ma L, Le Q, Zhi C, Liu P (2019) Deformation and fracture behaviors of AZ31B Mg alloy at elevated temperature under uniaxial compression. J Alloys Compd. 783:863–876. https://doi.org/10.1016/j.jallcom.2018.12.260
25. Galiyev A, Kaibyshev R, Gottstein G (2001) Correlation of plastic deformation and dynamic recrystallization in magnesium alloy ZK60. Acta Mater 49(7):1199–1207. https://doi.org/10.1016/S1359-6454(01)00020-9
26. Shang L, Jung IH, Yue S, Verma R, Essadiqi E (2010) An investigation of formation of second phases in microalloyed, AZ31 Mg alloys with Ca, Sr and Ce. J Alloys Compd. 492(1):173–183. https://doi.org/10.1016/j.jallcom.2009.11.159
27. Song G-L, Xu Z (2012) Effect of microstructure evolution on corrosion of different crystal surfaces of AZ31 Mg alloy in a chloride containing solution. Corros Sci 54:97–105. https://doi.org/10.1016/j.corsci.2011.09.005